Electronic Supplementary Information

A Cucurbituril/Polysaccharide/Carbazole Ternary Supramolecular Assembly for Targeted Cell Imaging

Xuan Wu,[a] Yong Chen,[a,b] Qilin Yu,[c] Feng-Qing Li,[a] Yu Liu*[,a,b]

[a] College of Chemistry, State Key Laboratory of Elemento-Organic Chemistry, Nankai University, Tianjin (300071), China. E-mail: yuliu@nankai.edu.cn.

[b] Collaborative Innovation Center of Chemical Science and Engineering (Tianjin), Tianjin (300071), China.

[c] Department of Microbiology, College of Life Sciences, Nankai University, Tianjin (300071), China

Table of Contents

1. Experimental Procedures

Materials. All reagents and solvents were obtained from commercial suppliers and were used as received, unless specified otherwise. All aqueous solutions were prepared with distilled water.

Purification and characterization techniques. Flash column chromatography was carried out with 200–300 mesh silica. ^{1}H NMR and ^{13}C NMR spectra were recorded on a Bruker DMX 400 MHz spectrometer. TEM images were obtained on a Tecnai G2F20 microscope (FEI) at an accelerating voltage of 200 kV. The samples were prepared by placing a drop of solution onto a carbon-coated copper grid and air-drying it. SEM images were obtained with a JSM-7500F scanning electron microscope. UV–vis spectra were recorded in a quartz cell (light path = 1 cm) on a Shimadzu UV-3600 spectrophotometer equipped with a PTC-348WI temperature controller. Fluorescence emission spectra were measured on a FLS 920P fluorescence spectrophotometer. Zeta potentials were measured with a Zeta PALS+BI-90 instrument (Brookhaven Co. USA). Fluorescence quantum yield were measured on a FLS920 instrument (Edinburg Instruments Ltd., Livingstone, UK) with a H_2 pulse lamp

MTT assay. The cells were seeded in 96-well plates at a density of 5×10^4 cells per well in 100 μL complete DMEM containing 10% fetal bovine serum, supplemented with 50 U·mL^{-1} penicillin and 50 U·mL^{-1} streptomycin, and cultured in 5% CO_2 at 37 °C for 24 h. Then the cells were exposed to serial solutions containing **G**, **CB[8]**, and the assembly, and further incubated for 12 h, respectively. After being irradiated under the white light, the cells were washed and replenished with fresh culture medium, and further incubated for 2 h. Subsequently, 10 μL of MTT solution was added into each cell and incubated for another 4 h. After that, the medium containing MTT was removed and dimethyl sulfoxide (DMSO, 75 μL) was added to each well to dissolve the MTT formazan crystals. Finally, the plates were shaken for 10 min, and the absorbance of formazan product was measured at 490 nm by a microplate reader (BioTek ELx808). Untreated cells in media were used as the blank control. All experiments were carried out with six replicates. The cytotoxicity was expressed as the percentage of the cell viability as compared with the blank control.

Colocalization experiment. The A549 cells were plated in 96-well plates at a density of 5×10^4 cells per well in 2.0 mL of complete culture medium for 24 h before treatment. Then cells were treated with **G⊂CB[8]** solution. For A549 cells, LysoTracker was directly added to the medium at a final concentration of 100 nM for 1 h to label lysosomes. The tumor cells were washed three times with fresh medium and investigated by fluorescence microscopy (IX-81, Olympus).

ROS generation. The ROS probes (H2DCF-DA and ABDA) were mixed with dyes, and irradiated under the high pressure mercury lamp (300 W) at the visible light regions respectively. Then the fluorescence or UV-vis spectra were recorded at intervals.

2. Synthesis of target molecules

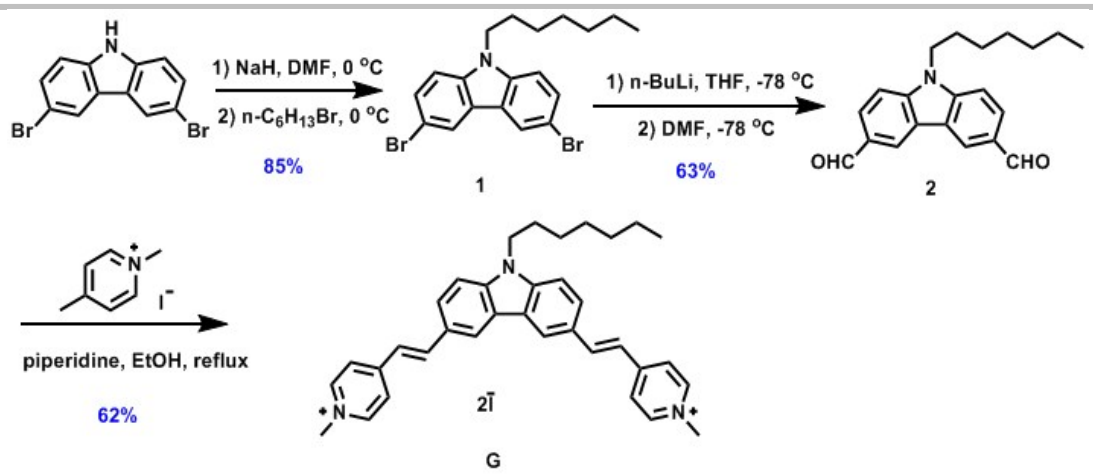

Scheme S1. Synthesis route of guest molecule **G**

1[1]: 60% NaH (0.16 g, 4 mmol) was added to the anhydrous DMF (25 mL) solution of 3,6-dibromo- 9*H*-carbazole (1.20 g, 3.7 mmol), and the mixture was balanced in the ice bath for 1h. Then 6-bromohexane (1.65 g, 10 mmol) was added and the mixture was stirred at 25 °C for 12h. Then, the mixture was poured to plenty of MeOH. After removing the solvent, the residue was dissolved in DCM (25 mL) and water (25 mL), the organic phase was separated and the aqueous phase was extracted by DCM (3 × 15 mL), then the combined organic phase was washed by saturated brine, dried over Na_2SO_4 and concentrated under reduced pressure. The crude product was purified by silica-gel chromatography (DCM/hexane = 1:1, *v/v*) to give compound **1** as a white solid (1.33 g, 85% yield). ^{1}H NMR (400 MHz, $CDCl_3$, 298 K) δ (ppm) = 8.18–7.18 (m, 2H), 7.62–7.47 (m, 2H), 7.30–7.17 (m, 2H), 4.23 (t, J = 6.9 Hz, 1H), 1.91–1.69 (m, 2H), 1.33–1.22 (m, 6H), 0.88–0.80 (s, 3H).

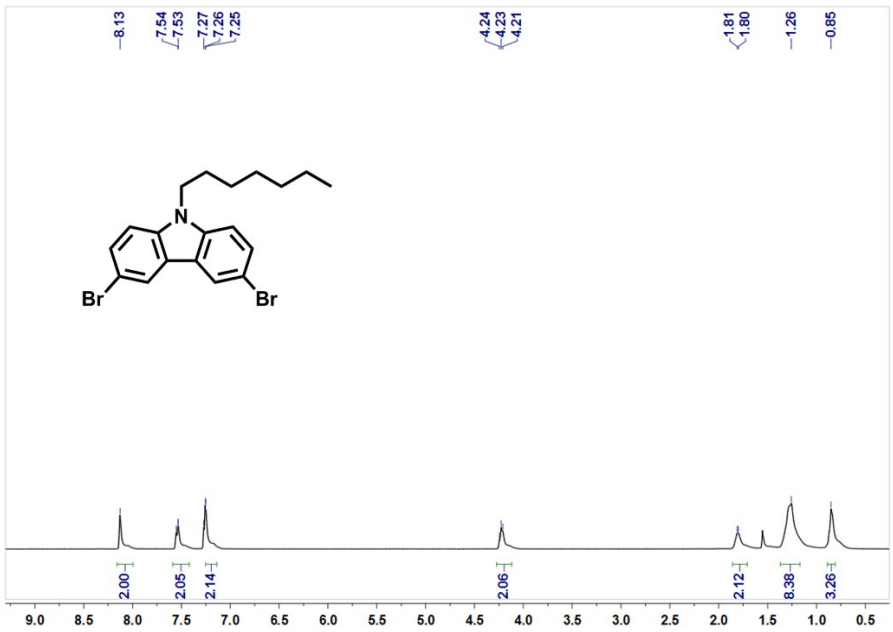

Figure S1. ^{1}H NMR spectrum of compound **1** (400 MHz, $CDCl_3$, 298 K).

2: *n*-BuLi solution in hexane (2.4 mM, 2.5 mL) was added into the **1** (1.27 g, 3.0 mmol) in anhydrous THF (20 mL) in the atmosphere of Ar at the temperature of -78 °C. Then the solution was stirred at this temperature for 30 min, followed by the addition of anhydrous DMF (3 mL). After that, the mixture was kept at this condition for another 1h.

Then the NH_4Cl solution was added to quench the reaction. After the removal of solvent, the crude product was purified by silica-gel chromatography (DCM/hexane = 2:1, *v/v*) to give the compound 2 as a white solid (0.61 g, 63% yield). ^{1}H NMR (300 MHz, DMSO-d_6, 298 K) δ (ppm) = 10.15 (s, 2H), 8.94 (d, J = 1.2 Hz, 2H), 8.12 (dd, J = 8.6, 1.5 Hz, 2H), 7.93 (d, J = 8.6 Hz, 2H), 4.57 (t, J = 7.1 Hz, 2H), 2.63–2.44 (m, 2H), 1.91–1.75 (m, 2H), 1.42–1.18 (m, 6H), 0.84 (t, J = 7.0 Hz, 3H)..

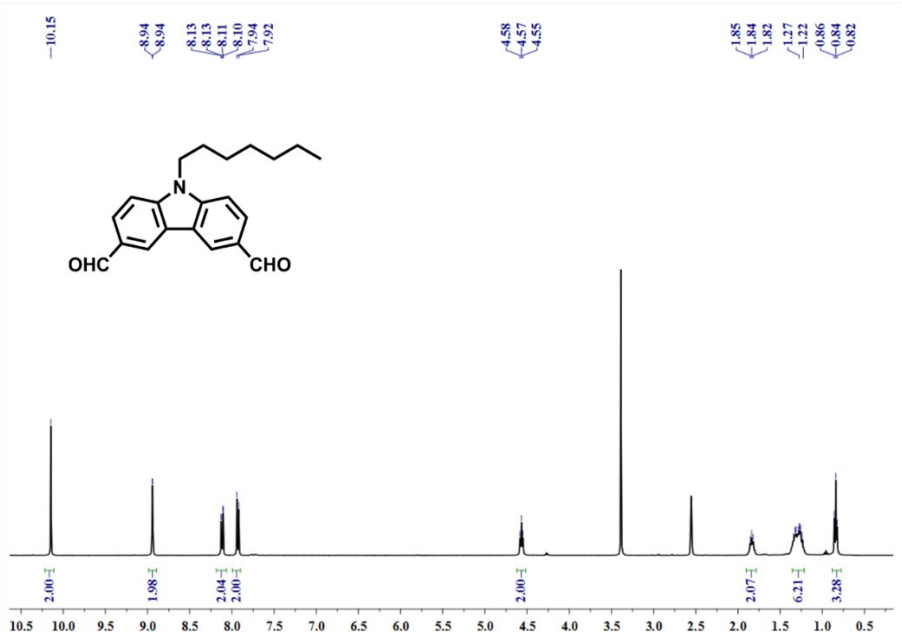

Figure S2. ^{1}H NMR spectrum of compound **2** (400 MHz, **DMSO**-d_6, 298 K).

G: Compound **2** (0.64 g, 2.0 mmol) and 1,4-dimethylpyridin-1-ium iodide (0.94 g, 4.0 mmol) were added into ethanol/DCM solution (15 mL, ethanol/DCM = 1:1, *v/v*), then three drops of piperidine was added under the refluxed condition. After being refluxed for 4h, the mixture was cooled to room temperature, the participate was collected and recrystallized in ethanol. The target molecule was obtained as dark red solid (2.19 g, 65% yield). ^{1}H NMR (400 MHz, DMSO-d_6, 298 K) δ (ppm): 8.84 (d, J = 6.8 Hz, 4H), 8.65 (s, 2H), 8.30–8.18 (m, 2H), 7.96 (d, J = 8.6 Hz, 2H), 7.81 (d, J = 8.7 Hz, 2H), 7.59 (d, J = 16.2 Hz, 2H), 4.49 (t, J = 6.9 Hz, 2H), 4.26 (s, 6H), 1.88–1.73 (m, 2H), 1.38–1.15 (m, 6H), 0.82 (t, J = 7.1 Hz, 3H). ^{13}C NMR (101 MHz, DMSO-d_6, 298 K) δ (ppm): 153.4, 145.4, 142.44, 142.42, 127.6, 127.2, 123.4, 123.1, 121.8, 121.1, 111.2, 47.2, 43.3, 31.4, 29.0, 26.5, 22.5, 14.3. HR-ESI-MS: m/z Calcd for $C_{35}H_{39}N_3^{2+}$ $[M-2I]^{2+}$ 250.6567, found 250.6490.

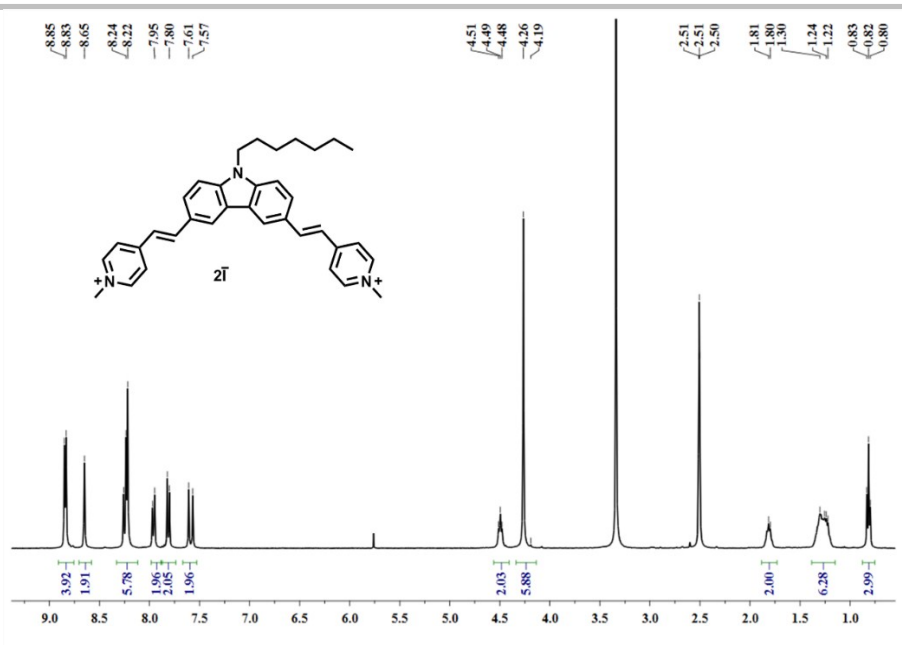

Figure S3. ^{1}H NMR spectrum of compound **G** (400 MHz, DMSO-d_6, 298 K).

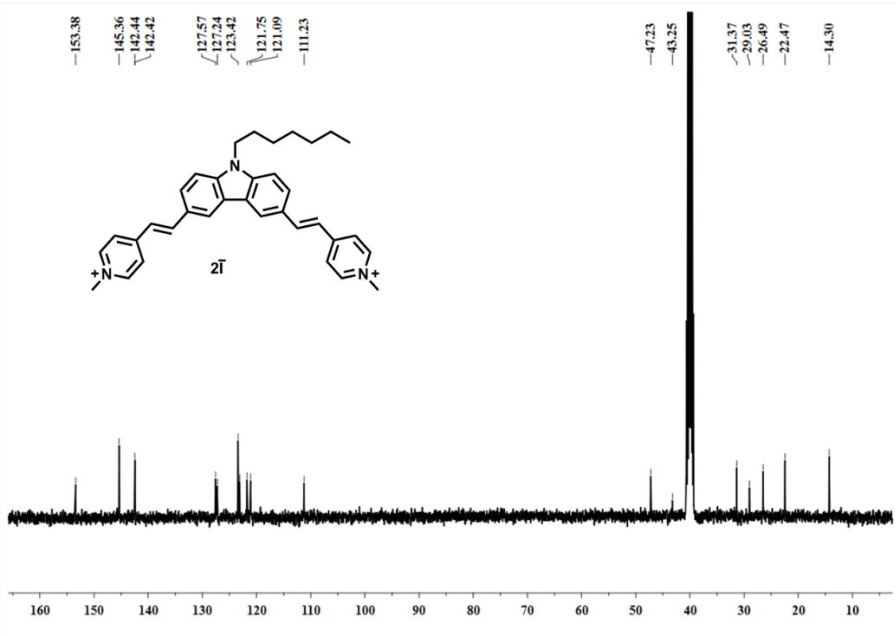

Figure S4. ^{13}C NMR spectrum of compound **G** (101 MHz, DMSO-d_6, 298 K).

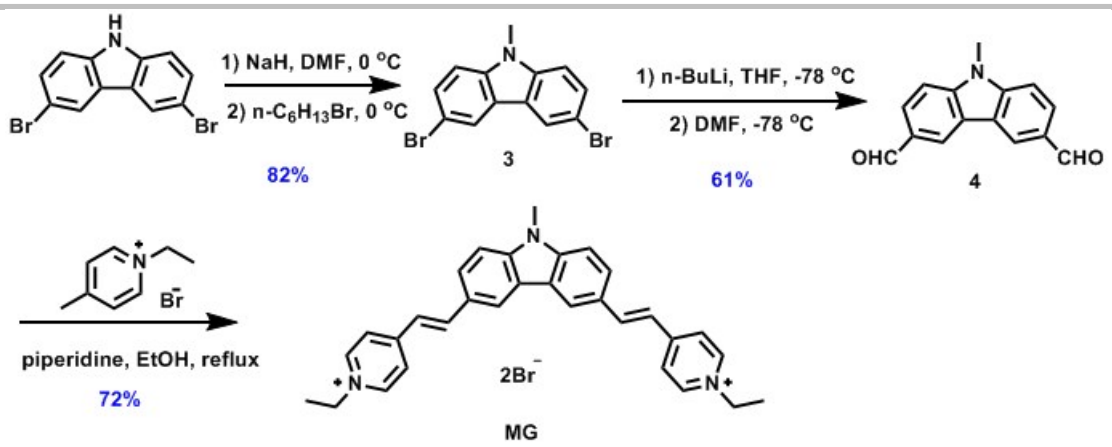

Scheme S2. Synthesis route of model guest molecule **G**

3[2]: 60% NaH (0.16 g, 4 mmol) was added to the anhydrous DMF (25 mL) solution of 3,6-dibromo- 9*H*-carbazole (1.20 g, 3.7 mmol), and the mixture was balanced in the ice bath for 1h. Then MeI (1.41 g, 10 mmol) was added and the mixture was stirred at 25 °C for 12 h. Then, the mixture was poured to plenty of MeOH. After removing the solvent, the residue was dissolved in DCM (25 mL) and water (25 mL), the organic phase was separated and the aqueous phase was extracted by DCM (3 × 15 mL), then the combined organic phase was washed by saturated brine, dried over Na_2SO_4 and concentrated under reduced pressure. The crude product was purified by silica-gel chromatography (DCM/hexane = 1:1, *v/v*) to give compound **3** as a white solid (1.11 g, 82% yield). ^{1}H NMR (400 MHz, DMSO-d_6, 298 K) δ (ppm): 8.52–8.41 (m, 2H), 7.66–7.56 (m, 4H), 3.87 (s, 3H).

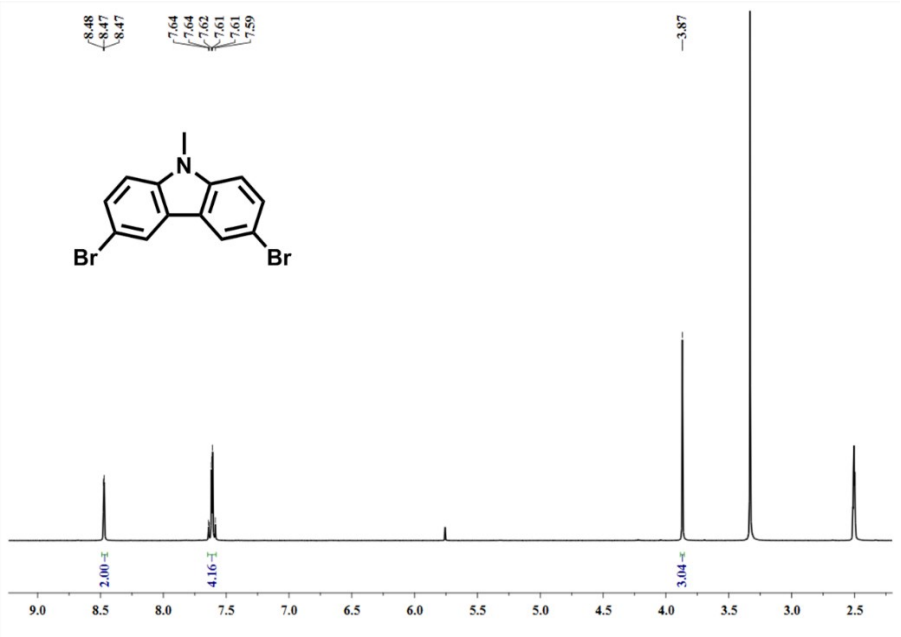

Figure S5. ^{1}H NMR spectrum of compound **3** (400 MHz, $CDCl_3$, 298 K).

4: *n*-BuLi solution in hexane (2.4 mM, 2.5 mL) was added into the **3** (1.01 g, 3.0 mmol) in anhydrous THF (20 mL) under the atmosphere of Ar at the temperature of -78 °C. Then the solution was stirred at this temperature for 30 min, followed by the addition of anhydrous DMF (3 mL). The mixture was kept at this condition for another 1h. After that, the NH_4Cl solution was added to quench the reaction. After the removal of solvent, the crude product was purified by

silica-gel chromatography (DCM/hexane = 2:1, *v/v*) to give the compound **4** as a white solid (0.43 g, 61% yield). ^{1}H NMR (300 MHz, DMSO-d_6, 298 K) δ (ppm): 10.17 (s, 2H), 8.70 (d, J = 1.5 Hz, 2H), 8.14 (dd, J = 8.5, 1.5 Hz, 2H), 7.59 (d, J = 8.5 Hz, 2H), 4.00 (s, 3H).

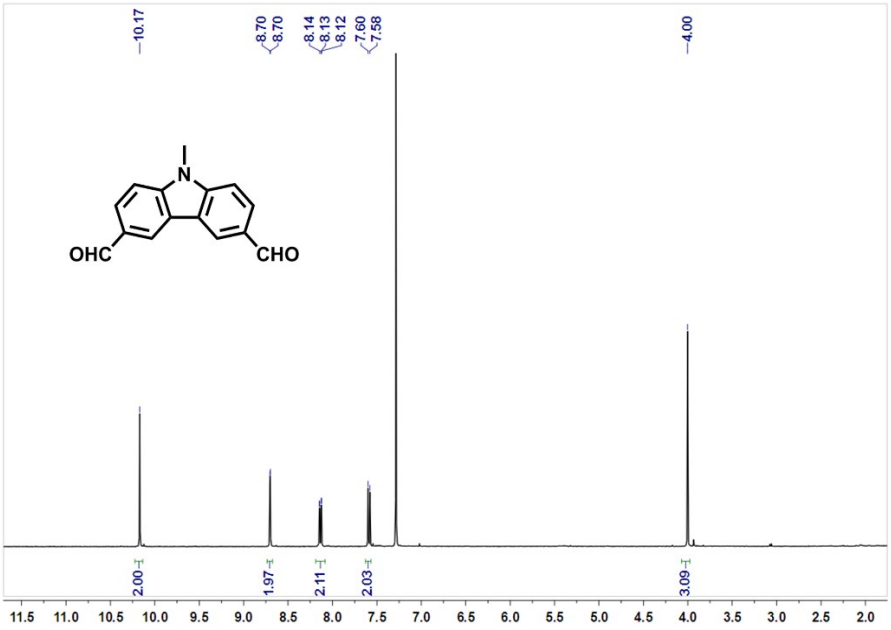

Figure S6. ^{1}H NMR spectrum of compound **4** (400 MHz, DMSO-d_6, 298 K).

MG: Compound **4** (0.47 g, 2.0 mmol) and 1-ethyl-4-methylpyridin-1-ium bromide (0.81 g, 4.0 mmol) were added into ethanol/DCM (15 mL, ethanol/DCM = 1:1, *v/v*), then three drops of piperidine was added under the refluxed condition. After the reaction for 4h, the mixture was cooled to room temperature, the participate was collected and recrystallized in ethanol. The target molecule was obtained as dark red solid (0.87 g, 72% yield). ^{1}H NMR (400 MHz, DMSO-d_6, 298 K) δ (ppm): 8.98 (d, J = 6.7 Hz, 4H), 8.63 (s, 2H), 8.32-8.20 (m, 6H), 7.99 (d, J = 8.6 Hz, 2H), 7.80 (d, J = 8.6 Hz, 2H), 7.60 (d, J = 16.2 Hz, 2H), 4.56 (q, J = 7.2 Hz, 4H), 3.99 (s, 3H), 1.55 (t, J = 7.3 Hz, 6H). ^{13}C NMR (101 MHz, DMSO-d_6, 298 K) δ (ppm): 153.7, 144.3, 143.0, 142.6, 127.6, 127.2, 123.8, 123.0, 121.8, 121.1, 111.0, 55.5, 30.1, 16.7. HR-ESI-MS: m/z Calcd for $C_{31}H_{31}N_3^{2+}$ $[M-2Br]^{2+}$ 222.6254, found 222.6256.

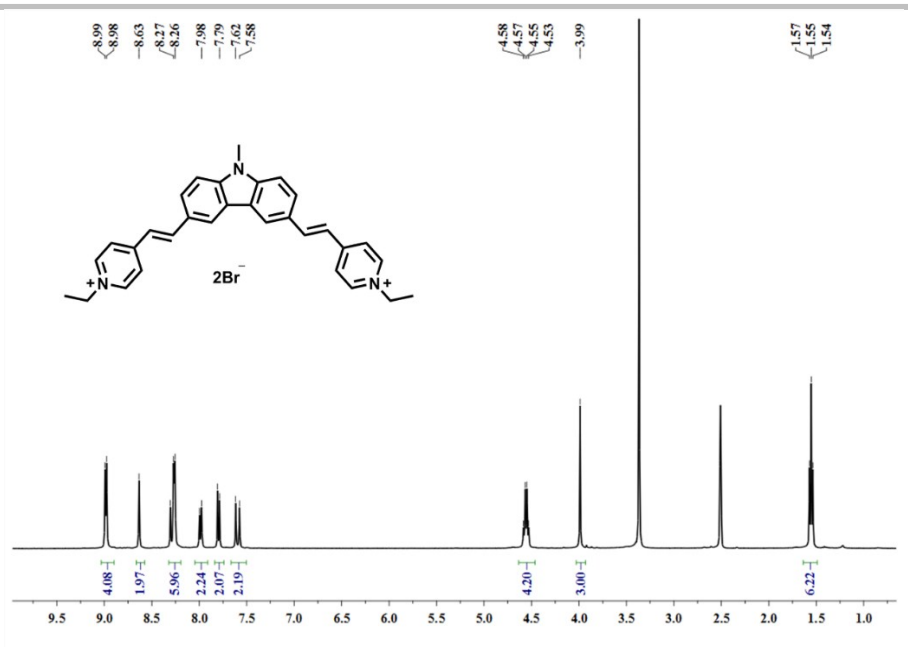

Figure S7. ^{1}H NMR spectrum of compound **MG** (400 MHz, DMSO-d_6, 298 K).

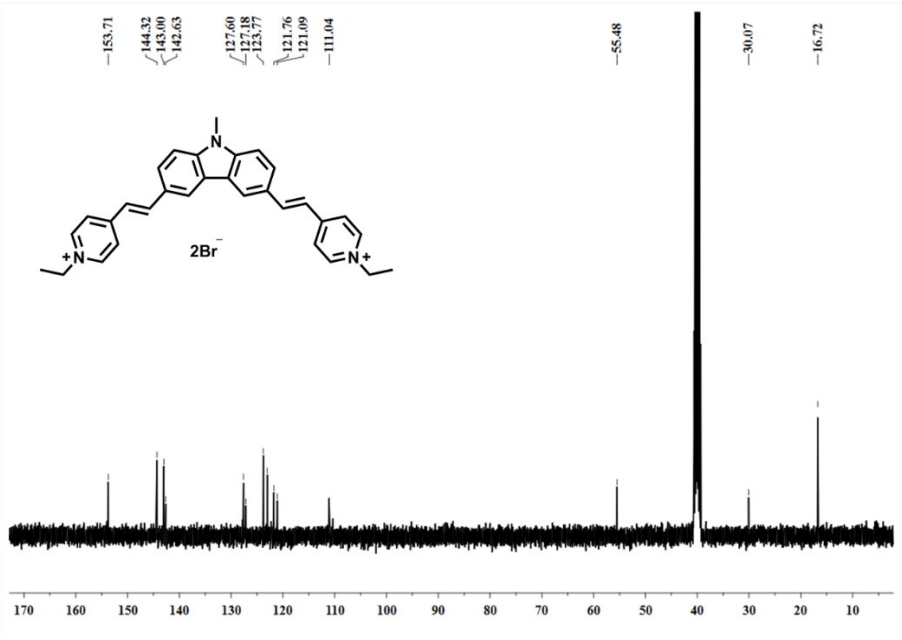

Figure S8. ^{13}C NMR spectrum of compound **MG** (101 MHz, DMSO-d_6, 298 K).

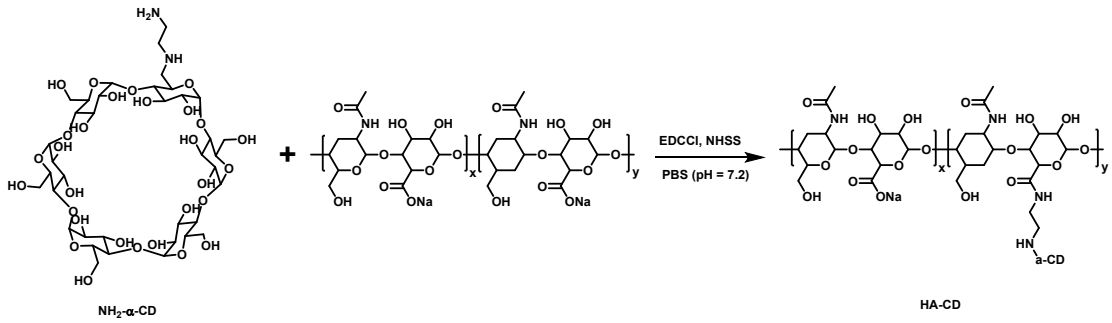

Scheme S3. Synthesis route of **HA-CD**

HA-CD: The sodium hyaluronate (100 mg, M_w = 150000) was dissolved into the PBS solution (50 mL, pH = 7.2), followed by the addition of EDCCl (168 mg, 0.88 mmol) and NHSS (190 mg, 0.88 mmol), and the solution was stired at room temperature for 30 min. Then the NH_2-α-CD (550 mg, 0.54 mmol) was added, and the mixture was stirred for another 24 h. finally, the solution was dialyzed against pure water for 5 days, and the target HA-CD was obtained as white solid (84 mg, 13% yield). ^{1}H NMR (400 MHz, D_2O, 298 K) δ(ppm): 5.03–4.94 (m, 6H), 4.54–4.31 (m, 18H), 3.99–2.98 (m, 130H), 2.81 (s, 7H), 1.92 (s, 27H).

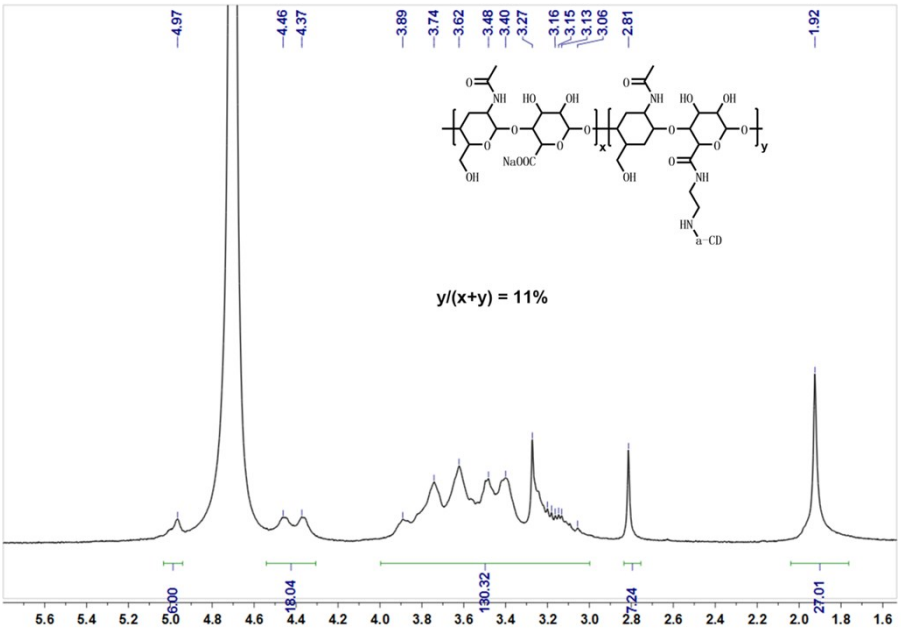

Figure S9. ^{1}H NMR spectrum of compound **HA-CD** (400 MHz, D_2O, 298 K)

3. Partial 2D NOESY spectrum of MG⊂CB[8]

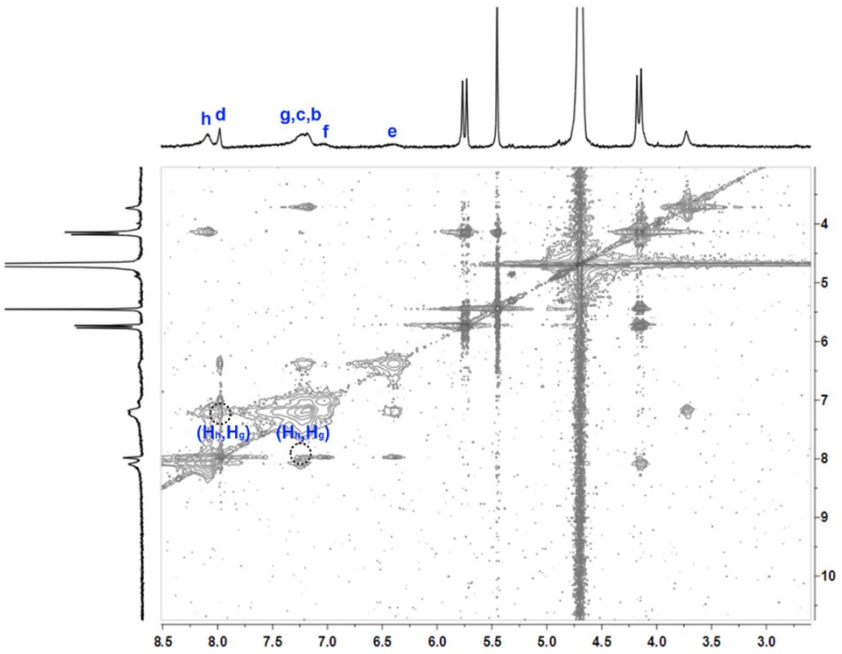

Figure S10. Partial 2D NOESY spectrum (400 MHz, 298 K, D_2O) of **MG⊂CB[8]** ([**CB[8]** = [**MG**] = 2 mM)

4. Job's plot for G⊂CB[8]

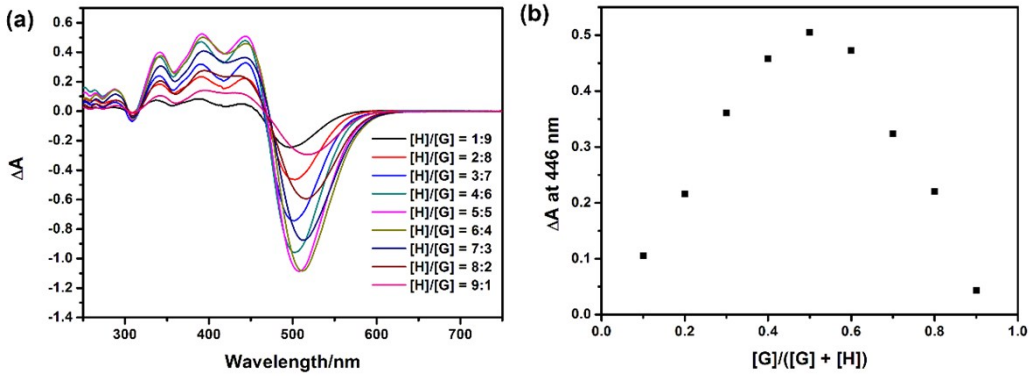

Figure S11. (a) Difference in the adsorption intensity of the mixture of **CB[8]** and **G** in water at different molar ratio while [**CB[8]**] + [**G**] = 2 × 10^{-5} M. (b) Job's Plot showing 1:1 stoichiometry of the complex between **CB[8]** and **G** by plotting the difference adsorption intensity at 446 nm against the molar fraction of **G** at an invariant total concentration of 2 × 10^{-5} M in aqueous solution.

5. Investigation of the binding constant between CB[8] and G

To determine the binding constant, UV-vis titration experiments were carried out in aqueous solution containing constant concentration of **G** (2 × 10^{-5} M) and varying concentration of **CB[8]**. The adsorption intensity changes of **G** upon the addition of **CB[8]** were measured and the binding constant was calculated from Eq.1.

$$\Delta A = (\Delta A_{\infty}/[G]_0)\ (0.5[H]_0 + 0.5([G]_0 + 1/K_a) - (0.5([H]_0^2 + (2[H]_0\ (1/K_a - [G]_0)) + (1/K_a + [G]_0)^2)^{0.5}) \quad \textbf{Eq.1}$$

Where ΔA is the adsorption intensity change of **G** at $[H]_0$, ΔA_{∞} is the adsorption intensity change of **G** when the guest is completely complexed, $[G]_0$ is the fixed initial concentration of the guest, and $[H]_0$ is the varying concentrations of the host. By non-linear fitting the spectrum data with Eq.1, the binding constant K_a was determined to be (3.38 ± 0.23) × 10^6 M^{-1}.

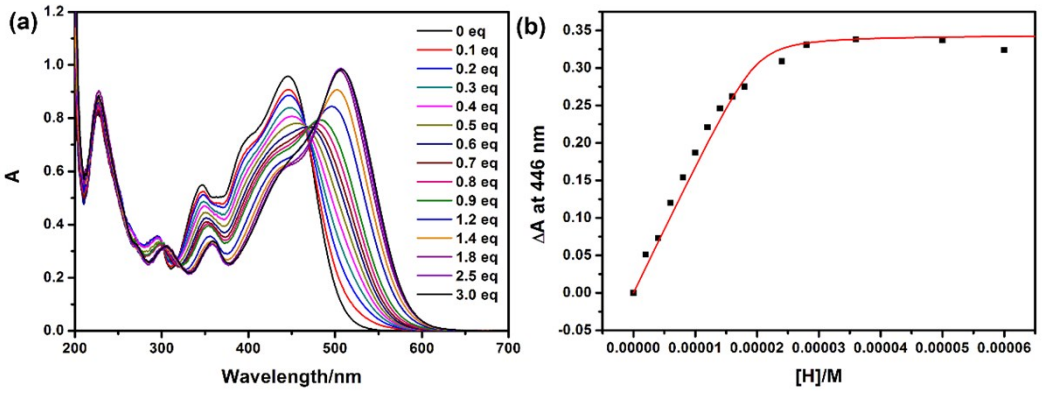

Figure S12. (a) UV-Vis spectra of **G** at a concentration of 2×10^{-5} M in aqueous solution upon the gradual addition of **CB[8]** from 1 to 3.0 eq., (b) the adsorption change of **G** at 446 nm upon the addition of **CB[8]** (0-6 × 10^{-5} M). The red solid curve was obtained from the nonlinear curve-fitting. (K = (3.38 ± 0.23) × 10^6 M^{-1})

6. 2D DOSY spectrum of MG⊂CB[8]

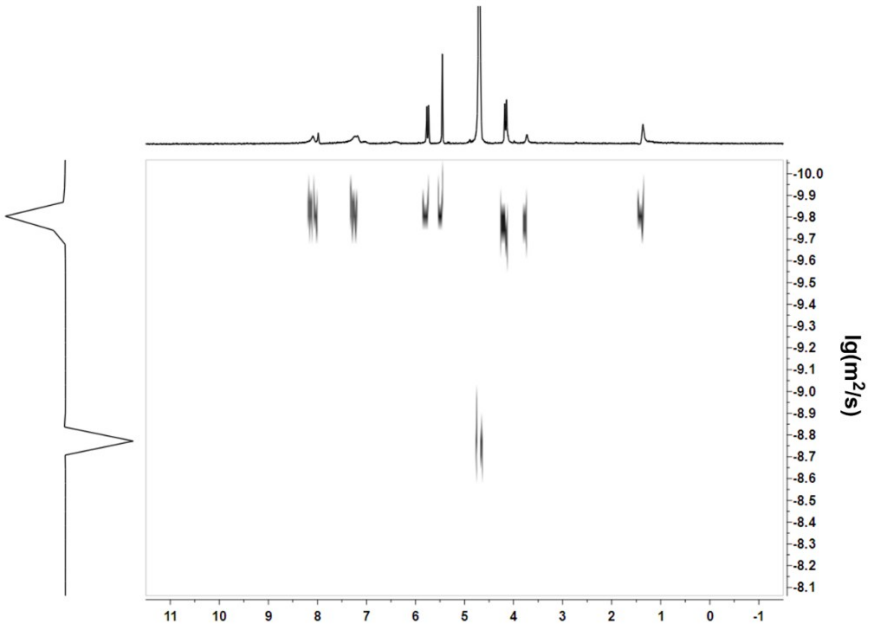

Figure S13. 2D DOSY spectrum (400 MHz, 298 K**,** D_2O) of **MG⊂CB[8]** ([**CB[8]**] = [**MG**] = 2 mM).

The hydrodynamic radius of **MG⊂CB[8]** in D_2O was calculated by the Stokes-Einstein relation (Eq. 2).

(Eq. 2)

Where *D* is the diffusion coefficient (obtained from Fig. S13), *k* is the Boltzmann constant (1.38×10^{-23} $m^2 \cdot kg \cdot s^{-2} \cdot K^{-1}$), *T* is the temperature in Kelvin (298 K), η is the viscosity of the solution (D_2O 8.95×10^{-4} $kg \cdot m^{-1} \cdot s^{-1}$), and *r* is the radius of the molecular sphere. The calculated results were listed in Table S1.

Table S1. The hydrodynamic radius of **MG⊂CB[8]** calculated from the DOSY experiment.

Sample	**MG⊂CB[8]**
lg D (lg $m^2 \cdot s^{-1}$)	-9.80
D ($m^2 \cdot s^{-1}$)	1.58×10^{-10}
r (nm)	1.54

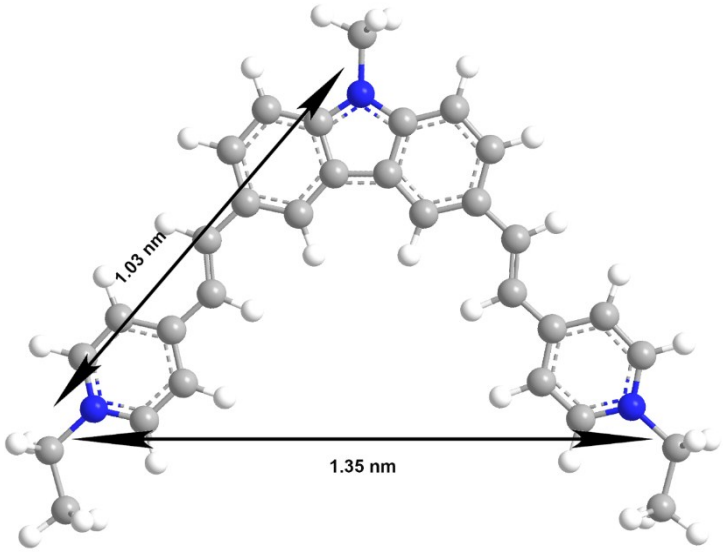

Figure S14. Geometry optimized structure of **MG** (Chem 3D, MM2).

7. Determination of the fluorescence lifetime of G and G⊂CB[8] in aqueous solution

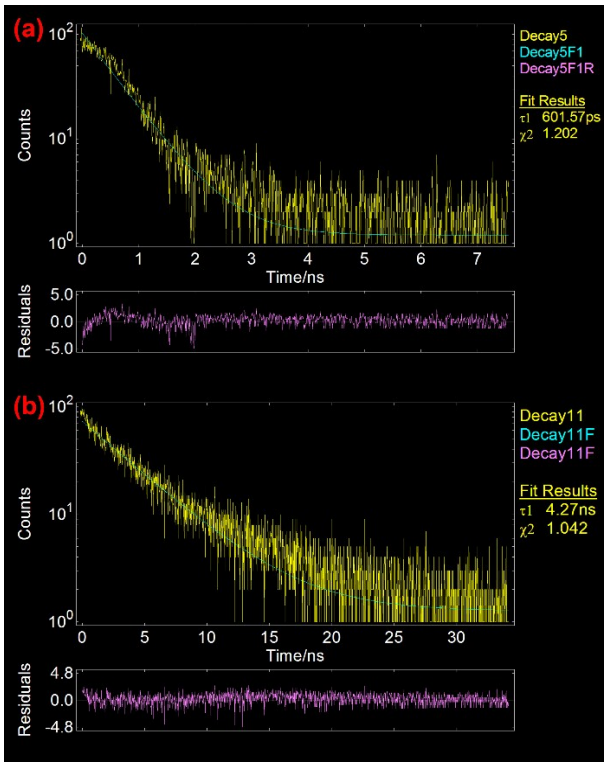

Figure S15. Fluorescence decay profiles of (a) **G** ([**G**] = 2 × 10^{-5} M**),** and (b) **G⊂CB[8]** ([**CB[8]**] = [**G**] = 2 × 10^{-5} M)

8. DLS and ξ-potential results of G and G⊂CB[8] in aqueous solution

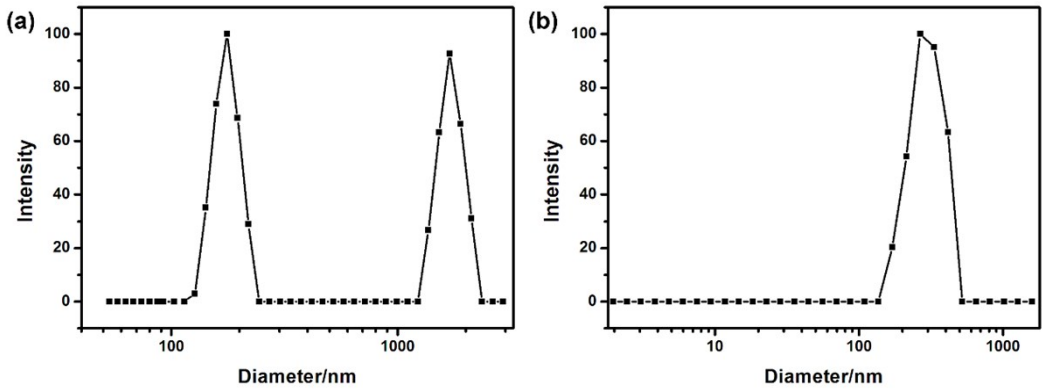

Figure S16. DLS results in aqueous solution of (a) **G**, and (b) **G⊂CB[8]**.

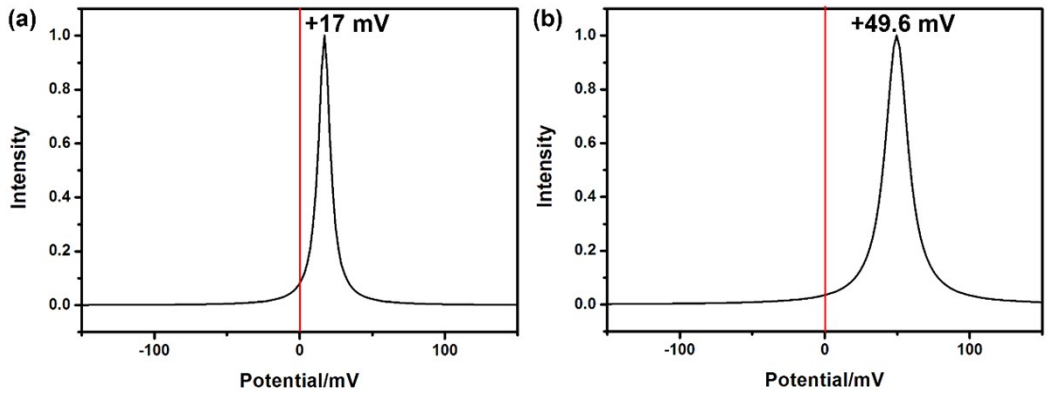

Figure S17. The measured ξ-potential results in aqueous solution of (a) **G**, and (b) **G⊂CB[8]**.

9. ROS and $^1O_2$ generation ability of G and G⊂CB[8]

As well known, this type of dipolar dyes containing the electron-donor and electron-accept motifs in one molecule has been widely studied in the potential application in the PDT. Moreover, the addition of **CB[8]** would restrict the intramolecular rotation, thus decreasing the non-radiative jump from the excited state, as well as stabilized the excited state, which would also facilitate the intersystem crossing efficiency for the generation of singlet oxygen ($^1O_2$) or other ROS. Herein, the 2′,7′-dichlorodihydrofluorescein diacetate (H2DCF-DA) was employed to evaluate the efficiency of ROS generation (Figure S18a), which undoubtedly played a critical role in PDT. As illustrated in figure S18a, H2DCF-DA was relatively stable under the irradiation of visible light, only a little increase in the fluorescence intensity was detected in 20 min. However, in the presence of **G**, it was observed the fluorescence became much stronger after the same time, indicating the generation of ROS to oxide the H2DCF-DA to H2DCF. The fluorescence became more stronger in the presence of **G⊂CB[8]**, indicating more ROS was generated. Moreover, another commercially available probe, 9,10-anthracenediyl-bis(methylene) dimalonic acid (ABDA), was used to verify the generation of $^1O_2$ in the process of light irradiation, which could be decomposed by the $^1O_2$ showing the changes in the absorbance. As depicted in figure S18b, after 5 min exposure of white light, 25% and 40% of ABDA were consumed in the presence of **G** and **G⊂CB[8]**, respectively. These phenomena certificated the addition of **CB[8]** would facilitate the intersystem crossing efficiency for the generation of $^1O_2$ for the potential application in PDT.

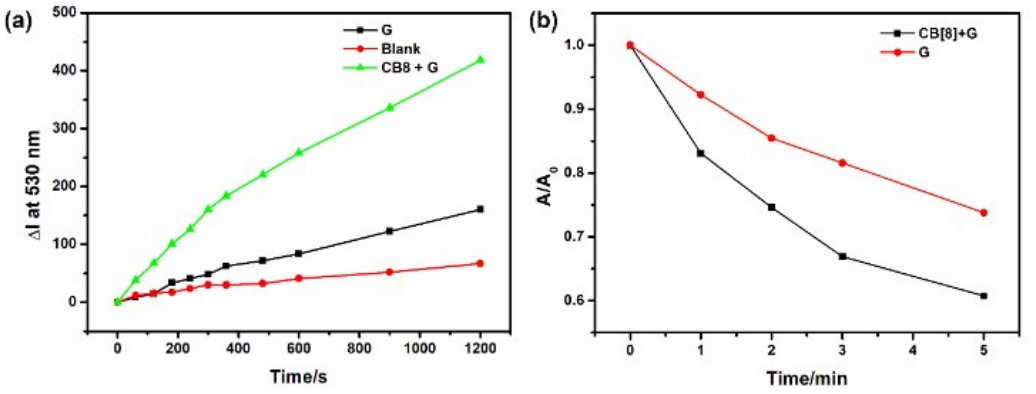

Figure S18. (a) ROS generation upon white light irradiation using H2DCF-DA as indicator ([**G**] = [**CB[8]**] = 2×10^{-6} M, [H2DCF-DA] = 4×10^{-5} M), (b) Decomposition rates of ABDA in the presence of PSs under light irradiation ([**G**] = [**CB[8]**] = 2×10^{-6} M, [ABDA] = 1×10^{-5} M).

10. Colocalization experiment of G⊂CB[8] in A549 cancer cells

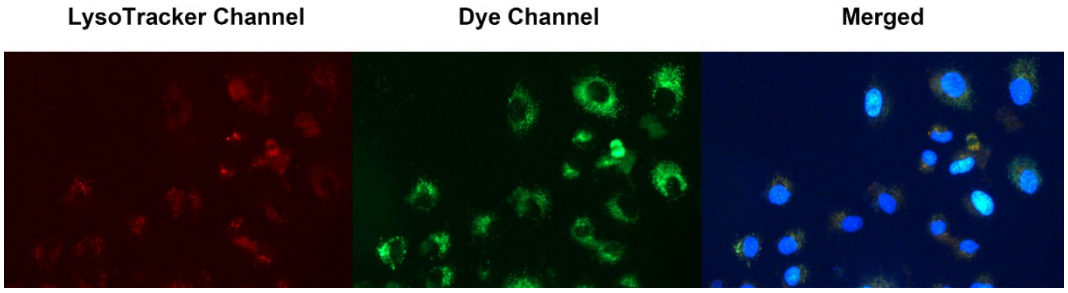

Figure S19. Confocal fluorescence images of A549 cells co-stained with **G⊂CB[8]**.

11. The A549 cell viability in the presence of G, CB[8], and G⊂CB[8]

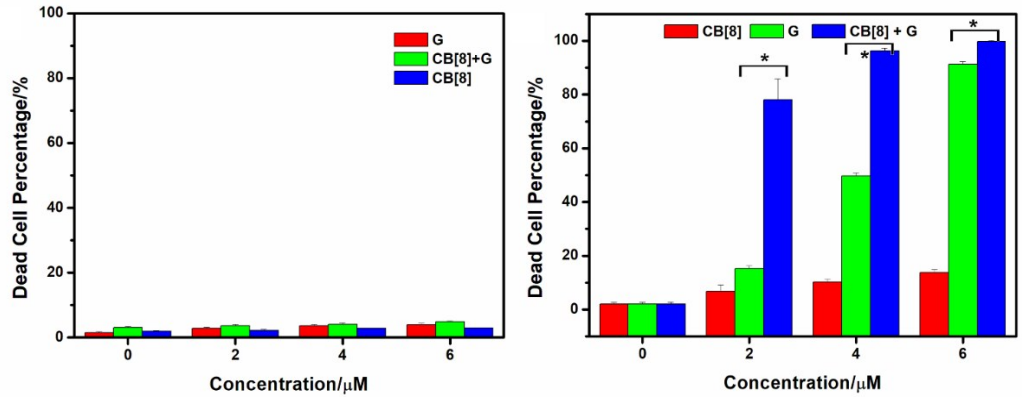

Figure S20. Anticancer activity of **G**, **CB[8]**, and **G⊂CB[8]** in A549 cancer cells, (b) in the dark environment, and (c) irradiated under the white light. ($P < 0.05$, *)

12. Study on the host-guest properties between G and α-CD

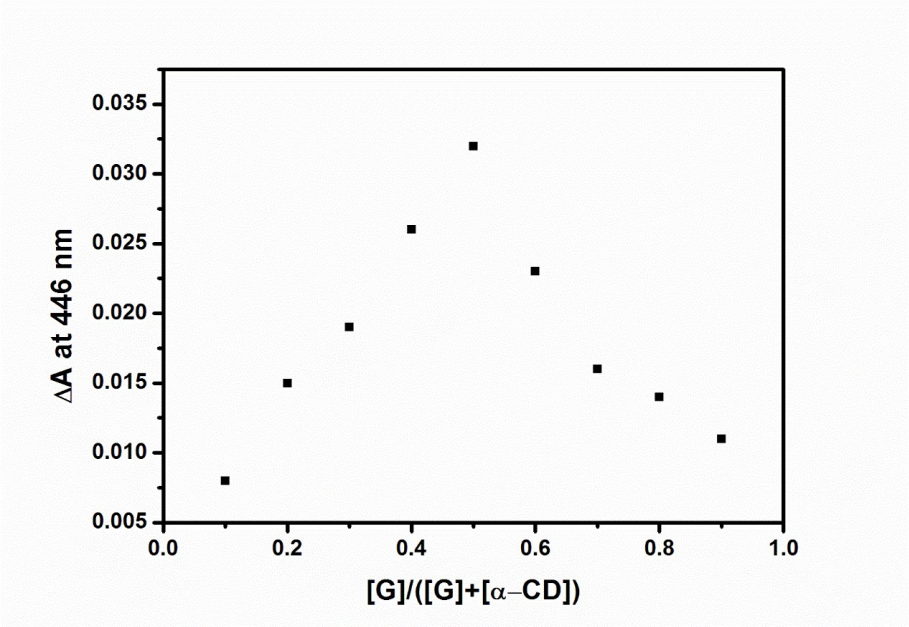

Figure S21. Job's Plot showing 1:1 stoichiometry of the complex between α-CD and **G** by plotting the difference adsorption intensity at 446 nm against the molar fraction of **G** at an invariant total concentration of 2×10^{-5} M in aqueous solution.

The binding affinity of **G** and α-CD was determined by the above mentioned method. That was to determine the adsorption intensity change of **G** upon the gradual addition of α-CD. By non-linear fitting the spectrum data with Eq.1, the binding constant K_a was determined to be $(5.9 \pm 0.4) \times 10^3$ M^{-1}.

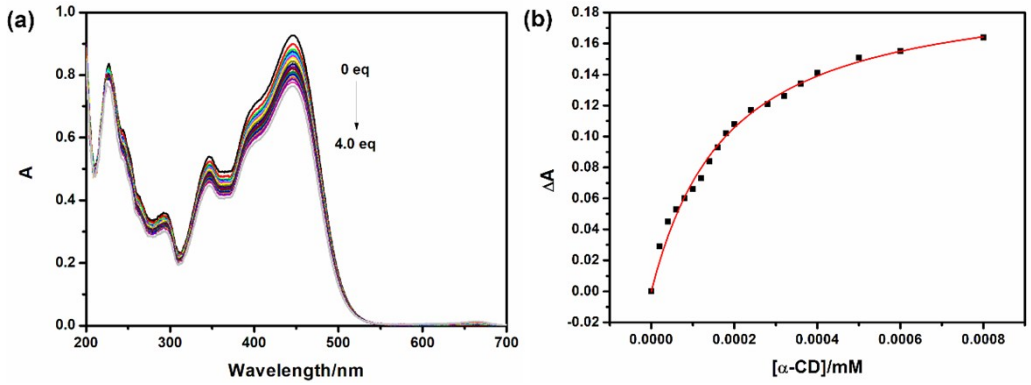

Figure S22. (a) UV-vis spectra of **G** at a concentration of 2×10^{-5} M in aqueous solution upon the gradual addition of α-CD from 1 to 4.0 eq., (b) the adsorption change of **G** at 446 nm upon the addition of α-CD ($0\text{-}8 \times 10^{-5}$ M). The red solid curve was obtained from the nonlinear curve-fitting. ($K = (5.9 \pm 0.4) \times 10^3$ M^{-1})

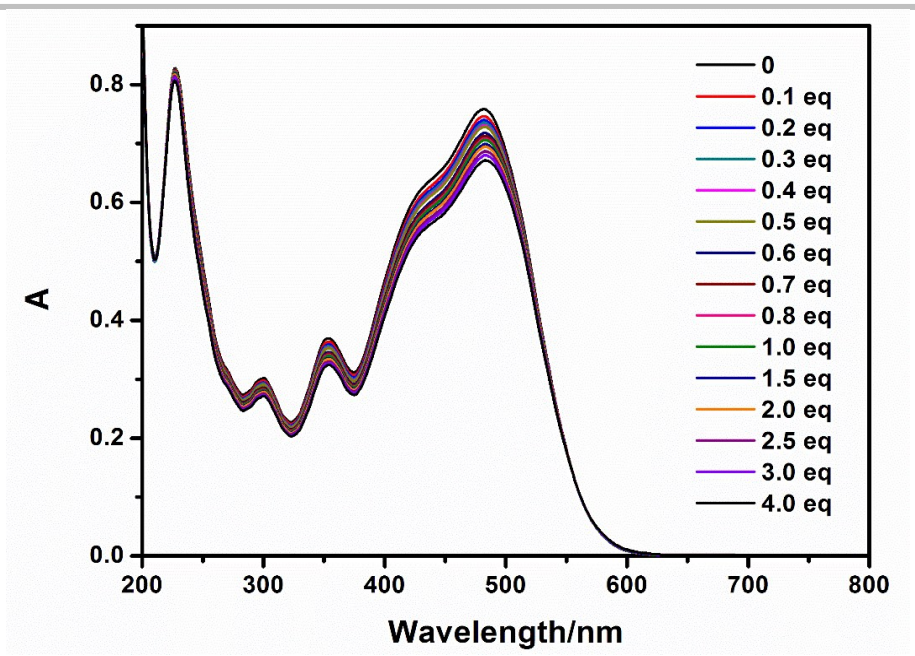

Figure S23. (a) UV-Vis spectra of **G⊂CB[8]** at a concentration ([**CB[8]**] = [**G**] = 2 × 10^{-5} M) in aqueous solution upon the gradual addition of α-CD from 1 to 4.0 eq.

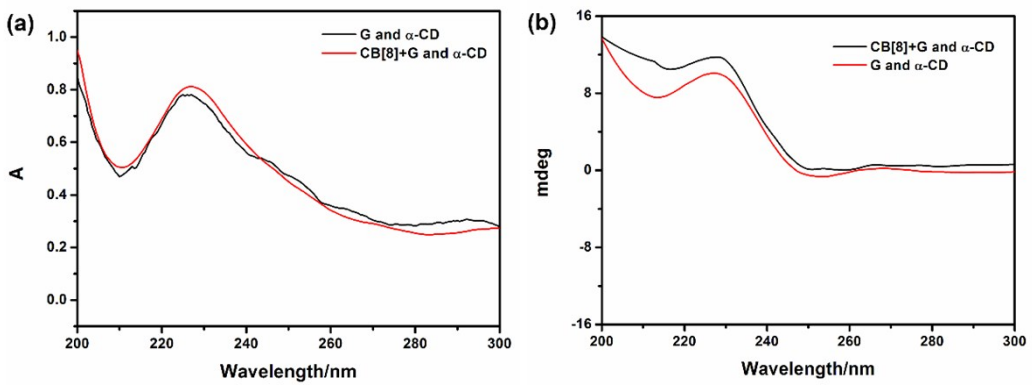

Figure S24. (a) partial UV-Vis spectra of **G** and **G⊂CB[8]** solution in the presence of α-CD ([**G**] = [**CB[8]**] = 2 × 10^{-5} M, [α-CD] = 8 × 10^{-5} M), (b) CD spectra of **G** and **G⊂CB[8]** solution in the presence of α-CD ([**G**] = [**CB[8]**] = 2 × 10^{-5} M, [α-CD] = 8 × 10^{-5} M).

13. UV-Vis and fluorescence spectra of G⊂CB[8] and HA-CD.

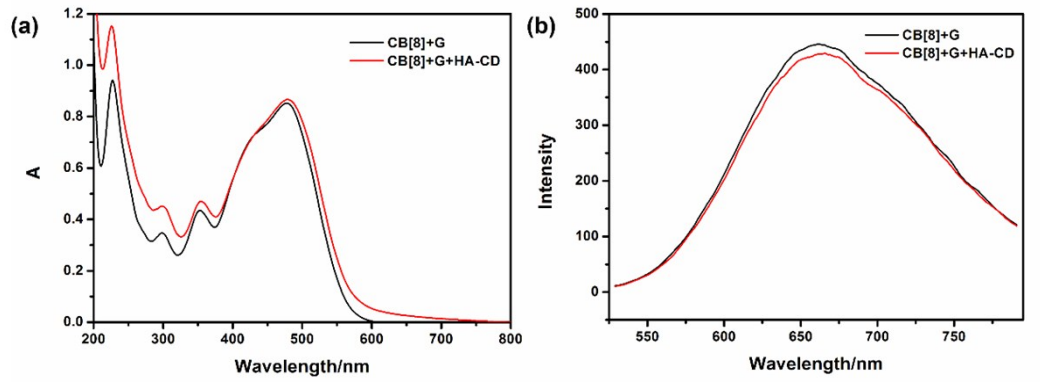

Figure S25. (a) UV-vis spectra of **G⊂CB[8]** in the presence and absence of **HA-CD** ([**CB[8]**] = [**G**] = 2 × 10^{-5} M, [**HA-CD**] = 0.008 mg/mL), (b) fluorescence spectra of **G⊂CB[8]** in the presence and absence of **HA-CD** ([**CB[8]**] = [**G**] = 2 × 10^{-5} M, [**HA-CD**] = 0.008 mg/mL).

14. TEM and SEM images of HA-CD@G⊂CB[8] and HA-CD.

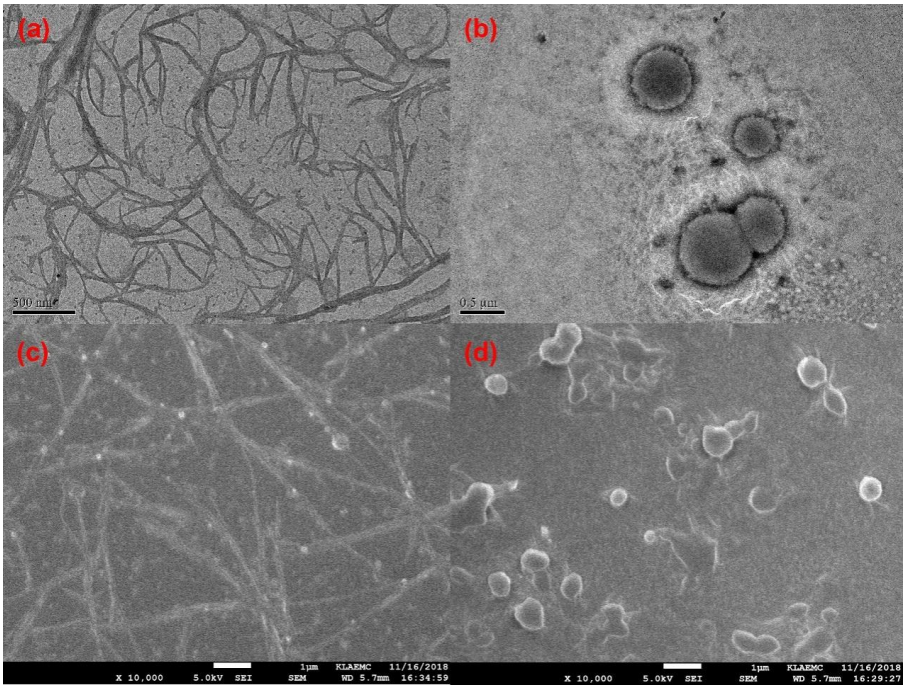

Figure S26. (a) and (c) TEM and SEM images of **HA-CD**, (b) and (d) TEM and SEM images of **HA-CD@G⊂CB[8].**

15. DLS and ξ-potential results of HA-CD@G⊂CB[8] in aqueous solution.

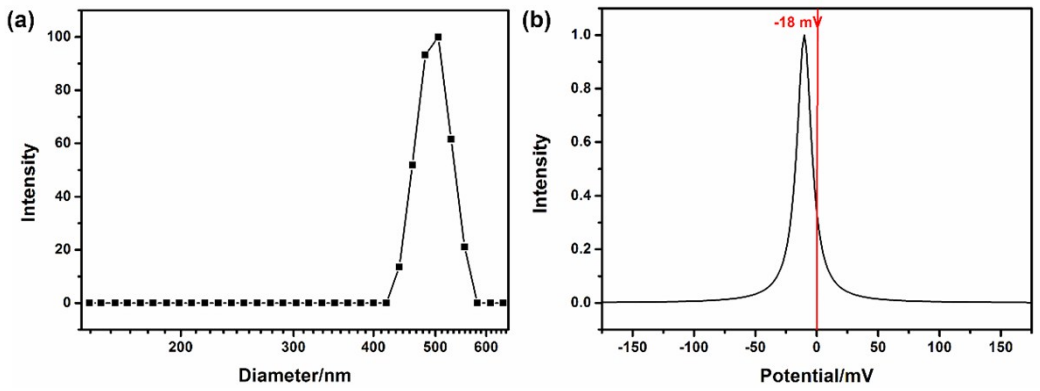

Figure S27. (a) DLS **result** of **HA-CD@G⊂CB[8]** in aqueous solution, (b) ξ-potential result of **HA-CD@G⊂CB[8]** in aqueous solution. ([**CB[8]**] = [**G**] = 2 × 10^{-5} M, [**HA-CD**] = 0.008 mg/mL).

16. ROS generation of HA-CD@G⊂CB[8] by using H2DCF-DA as the probe

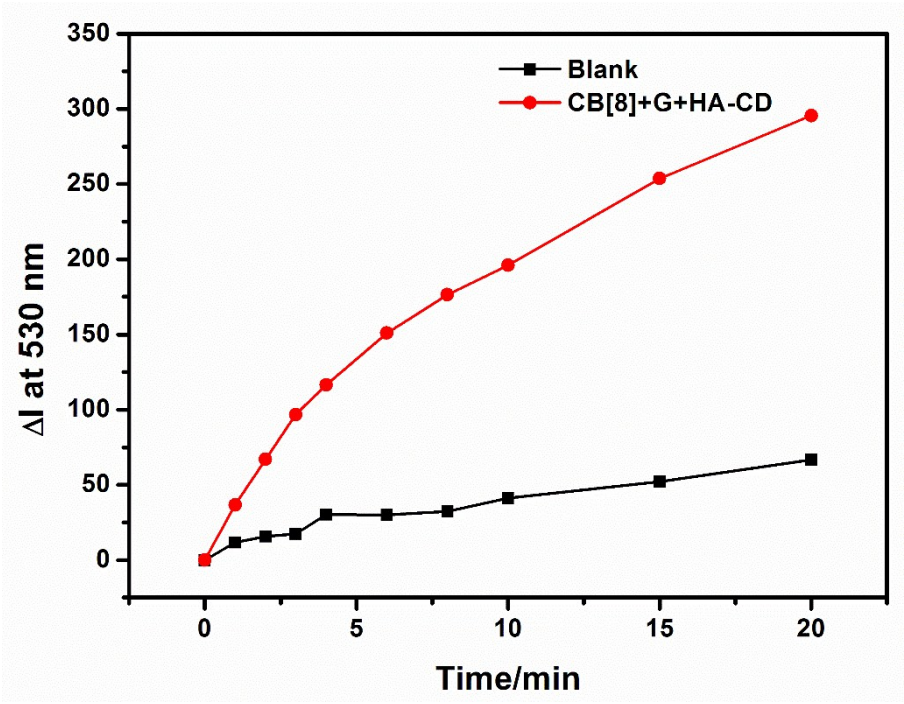

Figure S28. Time-dependant changes in the fluorescence intensity at 530 nm under the irradiation of white light. ([**CB[8]**] = [**G**] = 2 × 10^{-6} M, [**HA-CD**] = 8 × 10^{-4} mg/mL, [H2DCF-DA] = 4 × 10^{-5} M)

17. Cell images of 293T and A549 incubated with G⊂CB[8] and HA-CD@G⊂CB[8].

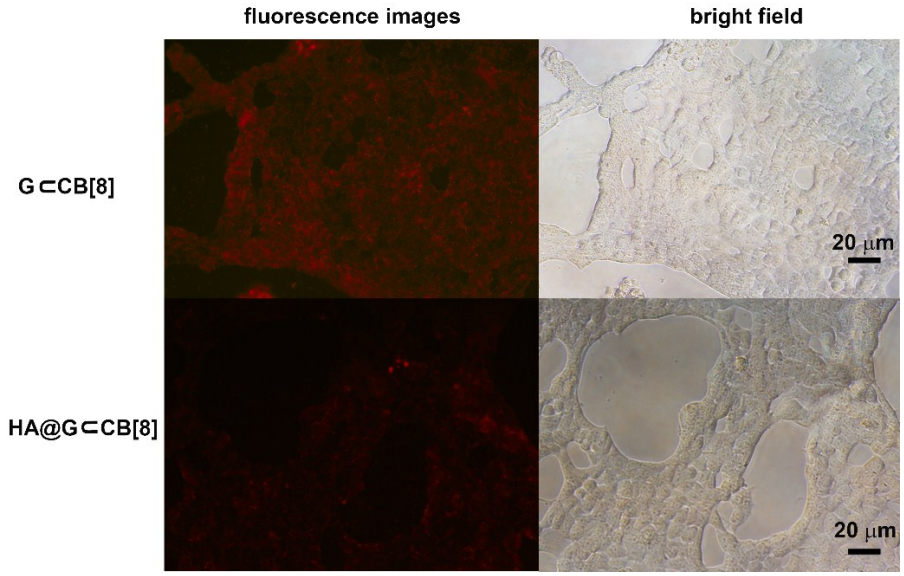

Figure S29. Cell images of 293T incubated with **G⊂CB[8]** and **HA-CD@G⊂CB[8]**.

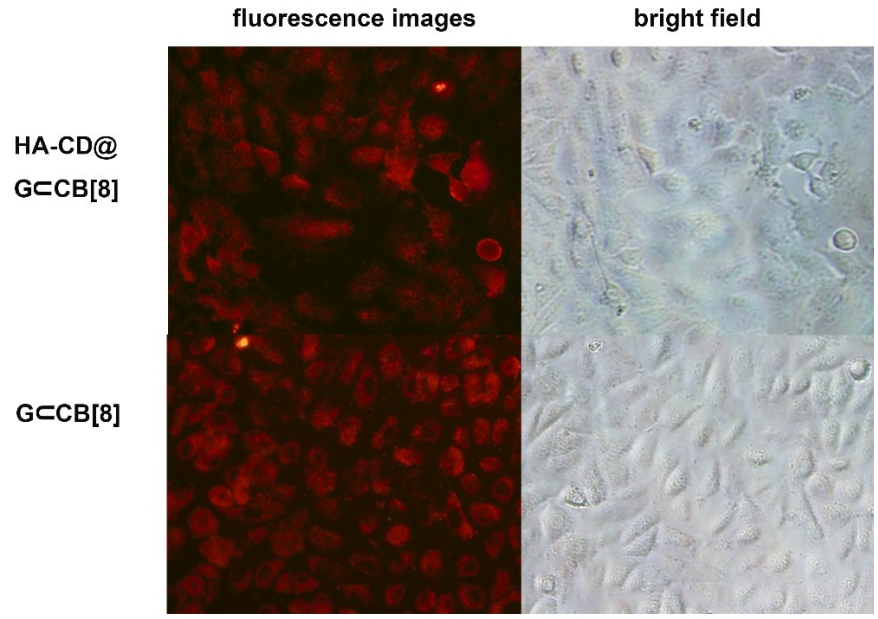

Figure S30. Cell images of 293T incubated with **G⊂CB[8]** and **HA-CD@G⊂CB[8]**

18. References

[1] M. Vetrichelvan, R. Nagarajan, S. Valiyaveettil, *Macromolecules*, 2006, **39**, 8303.

[2] K. Kawabata, M. Takeguchi, H. Goto, *Macromolecules*, 2013, **46**, 2078.

[3] M. Belloni, M. Manickam, Jon A. Preece, *Ferroelectrics*, 2002, **276**, 103.